

Hierarchical Open-Vocabulary 3D Scene Graphs for Language-Grounded Robot Navigation

Abdelrhman Werby^{1*}, Chenguang Huang^{1*}, Martin Büchner^{1*}, Abhinav Valada¹, and Wolfram Burgard²

Abstract—Recent open-vocabulary robot mapping methods enrich dense geometric maps with pre-trained visual-language features. While these maps allow for the prediction of point-wise saliency maps when queried for a certain language concept, large-scale environments and abstract queries beyond the object level still pose a considerable hurdle, ultimately limiting language-grounded robotic navigation. In this work, we present HOV-SG, a hierarchical open-vocabulary 3D scene graph mapping approach for language-grounded robot navigation. Leveraging open-vocabulary vision foundation models, we first obtain state-of-the-art open-vocabulary segment-level maps in 3D and subsequently construct a 3D scene graph hierarchy consisting of floor, room, and object concepts, each enriched with open-vocabulary features. Our approach is able to represent multi-story buildings and allows robotic traversal of those using a cross-floor Voronoi graph. HOV-SG is evaluated on three distinct datasets and surpasses previous baselines in open-vocabulary semantic accuracy on the object, room, and floor level while producing a 75% reduction in representation size compared to dense open-vocabulary maps. In order to prove the efficacy and generalization capabilities of HOV-SG, we showcase successful long-horizon language-conditioned robot navigation within real-world multi-storage environments. We provide code and trial video data at: <https://hovsg.github.io>.

I. INTRODUCTION

Humans acquire conceptual knowledge through multi-modal experiences. These experiences are paramount to object recognition and language as well as reasoning and planning [1], [2]. Cognitive maps store this information based on sensor fusion, fragmentation, and hierarchical structure. This is central to the human ability to navigate the physical world [3]–[5]. Recently, language proved to be an effective link between intelligent systems and humans and can enable robot autonomy in complex human-centered environments [6]–[13].

Classical methods for robot navigation build dense spatial maps of high accuracy using approaches to simultaneous localization and mapping (SLAM) [14], [15]. Those give rise to fine-grained navigation and manipulation based on geometric goal specifications. Recent advances have combined dense maps with pre-trained zero-shot vision-language models, which facilitates open-vocabulary indexing of observed environments [6]–[10], [16], [17]. While these approaches marry the area of classical robotics with modern open-vocabulary semantics, representing larger scenes while

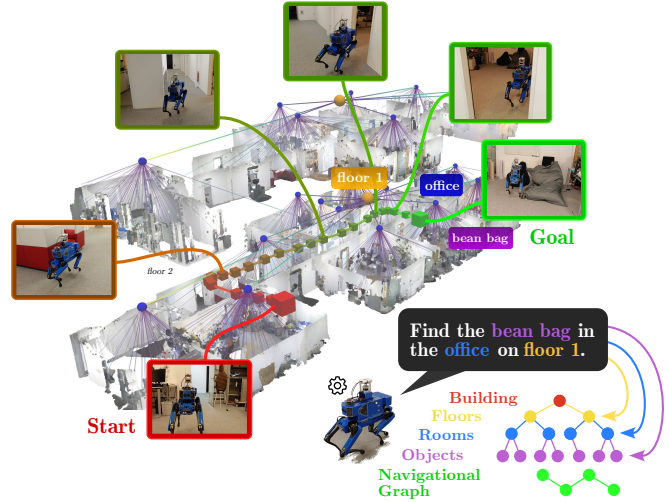


Fig. 1: HOV-SG allows the construction of accurate, open-vocabulary 3D scene graphs for large-scale and multi-story environments and enables robots to effectively navigate in them.

abstracting still poses a considerable hurdle. Scalable scene representations generated from real-world perception inputs should generally fulfill the following requirements: 1) Object-centricity and abstraction in terms of hierarchies, 2) efficiency regarding storage capacity as well as efficacy in terms of actionability, 3) true open-vocabulary indexing and simple querying.

A number of works approach this using 3D scene graph structures [15], [18], [19] that excel at representing larger environments efficiently. At the same time, they constitute a useful interface to semantic tokens used for prompting large language models (LLM). Nonetheless, most approaches rely on closed-set semantics with the exception of Concept-Graphs [11] that focuses on smaller scenes.

In this work, we present **Hierarchical Open-Vocabulary 3D Scene Graphs**, short HOV-SG. Our approach abstracts from dense panoptic maps and allows indexing of three distinct concepts, namely floors, rooms as well as objects. We utilize open-vocabulary vision-language models [20], [21] across all concepts in order to construct 3D scene graph hierarchies that span multi-story environments while maintaining a small memory footprint. Given its concept-centric nature, the HOV-SG representation is promptable using LLMs. Different from previous work, our approach relates to different conceptual levels by first decomposing abstract queries such as “*towel in the bathroom on the upper floor*” and scoring the obtained tokens against the different levels

* Equal contribution.

¹ Department of Computer Science, University of Freiburg, Germany.

² Department of Eng., University of Technology Nuremberg, Germany.

Supplementary material can be found at <https://hovsg.github.io>. This work was funded by the German Research Foundation (DFG) Emmy Noether Program grant number 468878300, the BrainLinks-BrainTools Center of the University of Freiburg, and an academic grant from NVIDIA.

of the hierarchy. We complement this with a navigational Voronoi graph that covers multiple floors including stairs, which allows actionable grounding of decomposed queries in the environment. This enables object retrieval and long-horizon robotic navigation in large-scale indoor environments from abstract queries as shown in Fig. 1.

As part of this work, we present state-of-the-art results in open-set 3D semantic segmentation, object retrieval from long queries as well as robust semantic room classification from perception inputs. In addition, we propose a novel open-vocabulary semantic similarity metric termed AUC_k^{top} . It measures the area under the top-k accuracy curve and thus scales to very large numbers of object categories and to differently-sized label sets used for evaluation. In summary, we make the following main contributions:

- We introduce a pipeline for constructing hierarchical, open-vocabulary 3D scene graphs from multi-story environments that enables LLM-based prompting, planning as well as robotic navigation.
- We extensively evaluate our approach across three diverse datasets as well as a real-world environment. We achieve state-of-the-art results in 3D open-set semantic segmentation and demonstrate successful robotic navigation from abstract language queries.
- We introduce a novel evaluation metric for measuring open-vocabulary semantics termed AUC_{top-k} and publish code at <https://hovsg.github.io>.

II. RELATED WORK

A. Semantic 3D Mapping

Enriching a geometric map with semantic information is a stepping stone to a flexible and versatile navigation system [4], [6], [7], [16], [22], [23]. In the past, researchers created semantics-enhanced or instance-level maps by learning sensor observation features [24], matching pre-built object shapes to the geometric map [25], back-projecting 2D semantic predictions into the 3D space [26]–[28], or instantiating 2D detections with basic 3D elements such as cubes or quadrics [29], [30]. These methods have shown their capabilities of reconstructing scenes with both accurate geometric structure and precise semantic meaning. However, most of these methods only work with a fixed category set constrained by either the trained semantic prediction models or the pre-defined set of relevant object primitives.

On account of recent advancements in large vision-language models such as CLIP [20] and their fine-tuned counterparts, a number of works proposed map representations that integrate visual-language features into geometric maps, enabling open-vocabulary indexing of objects [7]–[10], [16], [17], [31], audio data [10], [16] and images [16], [22] in an unstructured environment. While lifting the constraints of fixed semantic categories, these approaches often necessitate the storage of a visual-language embedding for each geometric element such as points, voxels, or 2D cells in the map, resulting in a significant increase in storage overhead.

B. 3D Scene Graphs

3D scene graphs have emerged as an effective, object-centric representation of large-scale indoor [18], [19], [32] and outdoor scenes [15]. By representing objects or spatial concepts as nodes and their relations as edges, 3D scene graphs allow to efficiently represent larger scenes [15], [18], [32]. Both edges and nodes can hold geometric and semantic attributes, which are often inferred from certain off-the-shelf networks [33]. Decomposing scenes into objects and their relations enables higher-level reasoning for robotic navigation and manipulation. This is particularly useful in the realm of reasoning, planning, and navigation given the object-centric nature of these tasks [18], [34], [35]. Often combined with odometry estimates from simultaneous localization and mapping (SLAM) [15], [36], [37], 3D scene graphs also allow a tight coupling between semantics and highly accurate mapping approaches utilizing e.g. meshes to represent environments [18].

Early works have shown how to encode hierarchies via abstraction in both the spatial and the semantic domain using offline approaches [19], [32]. Successive works investigated learning-based scene graph construction [33], [38] as well as dynamic indoor scenes [18]. Several approaches such as SceneGraphFusion [33] and S-Graphs [36] also investigate the real-time capabilities of their proposed approaches. Most recently, ConceptGraphs [11] was the first to show how to combine 3D scene graphs with open-vocabulary vision-language features. In addition, the authors show how to query the graph using LLMs and demonstrate interesting application scenarios.

Conceptually, our work is most similar to ConceptGraphs and Hydra. While ConceptGraphs is only evaluated on small scenes and mostly validated by human evaluators in terms of semantic accuracy of nodes etc. Different from ConceptGraphs and similar to Hydra [18], which does not operate on open-vocabulary features, our approach demonstrates how to efficiently represent actionable, hierarchical 3D scene graphs that are attributed with open-vocabulary features. These scene graph hierarchies span entire multi-story environments and allow robotic navigation and search from abstract queries. In addition to this, we outperform ConceptGraphs in terms of 3D semantic segmentation accuracy and make contributions regarding the open-vocabulary semantic classification of room types. Moreover, the proposed open-vocabulary graph representation of the environment is considerably more memory efficient by consuming an average of 75% less storage compared to previous dense open-vocabulary representations while preserving extensive semantic information.

III. TECHNICAL APPROACH

This work aims to develop a concise and efficient visual-language graph representation for large-scale multi-floor indoor environments given RGB-D observations and odometry. The graph should facilitate the indexing of semantic concepts through natural language queries and enable robotic navigation in multi-floor environments. We address this by proposing

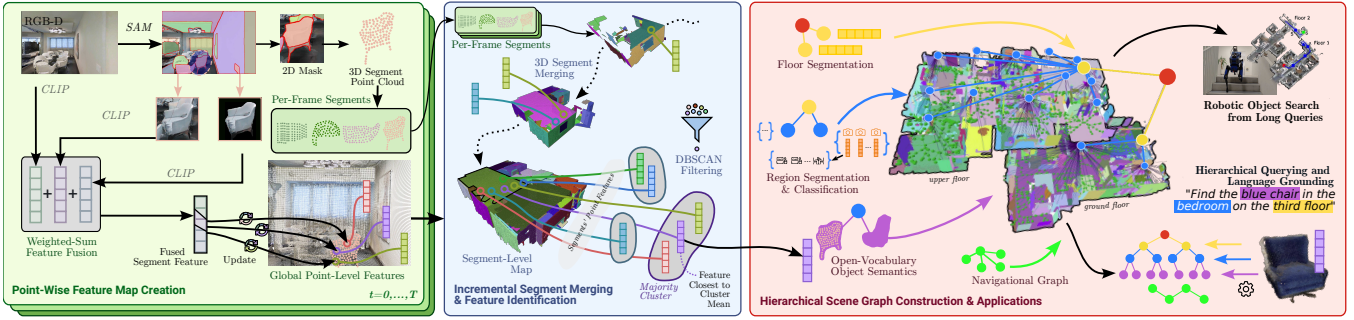


Fig. 2: HOV-SG builds hierarchical open-vocabulary 3D scene graphs of indoor household scenes. We first use SAM to extract object masks per frame while obtaining vision-language features via CLIP. In the next step, we aggregate these features on a point level in the map. Secondly, we segment the full point cloud based on merged 3D masks. To produce more meaningful semantic object features, we employ a DBSCAN-based filtering approach to obtain a majority vote feature for each object. To construct an actionable 3D scene graph, we segment the obtained panoptic map into multiple floors, segment and classify distinct regions using several view embeddings, and identify object names via querying. As a result, HOV-SG allows hierarchical querying and navigation using mobile robots even in complex multi-floor environments.

Hierarchical Open-Vocabulary Scene Graphs, in short HOV-SG. In the following, we describe (i) the construction of a 3D segment-level open-vocabulary map (Sec. III-A), (ii) the generation of the hierarchical open-vocabulary scene graphs (Sec. III-B), and (iii) language-conditioned navigation across large-scale environments (Sec. III-C). Fig. 2 presents an overview of our method.

A. 3D Segment-Level Open-Vocabulary Mapping

1) *Frame-Wise 3D Segment Merging*: Given a sequence of RGB-D observations, we utilize Segment Anything [21] to obtain a list of class-agnostic 2D binary masks at each timestep. The pixels in each mask are then backprojected to 3D using the depth information, resulting in a list of point clouds, or 3D segments. Based on accurate odometry estimates, we transform all 3D segments into the global coordinate frame. These frame-wise segments are either initialized as new global segments or merged with existing ones based on an overlap metric:

$$R(m, n) = \max(\text{overlap}(S_m, S_n), \text{overlap}(S_n, S_m)), \quad (1)$$

where S_m and S_n indicate segment (or point cloud) m and n , $\text{overlap}(S_a, S_b)$ is computed by taking the number of points in S_a showing a neighbor in S_b within a certain distance divided by the total number of points in S_a . Different from Gu *et al.* [11], who incrementally merge new segments with one global segment that has the largest overlapping ratio, we construct a graph with edge weights according to the corresponding overlapping ratios. Based on these weights, highly-connected subgraphs are subsequently merged. In this way, one segment can merge with more segments, which is useful in situations in which an incoming segment is, e.g., filling a gap between two already registered global segments.

2) *Open-Vocabulary Segment Features*: For each obtained 2D SAM mask per frame, we obtain an image crop based on its bounding box as well as an image of the isolated mask without background. We encode the full RGB frame and the two mask-wise images with CLIP [20] and fuse them in a weighted-sum manner, see Fig. 2. Previous work [39] proposed to use the CLIP feature of the masked image without

background, while others [10] approach this by combining the CLIP features of the whole image and the target mask’s crop including background. In our work, we empirically show that encoding the full RGB frame and the two mask-wise images with CLIP and fusing them in a weighted-sum manner achieves improved results. The fusion scheme can be formulated as:

$$f_i = w_g f_g + w_l f_l + w_m f_m, \quad (2)$$

where f_i indicates the fused features for the i -th 2D mask in the frame, f_g , f_l , and f_m indicate the CLIP features extracted from the entire RGB frame, the image crop of the 2D mask, and the image crop of the 2D mask excluding the background, respectively. Furthermore, w_g , w_l , and w_m represent their respective weights, which sum up to 1.

Assuming a single CLIP feature for each mask, we transform the 2D mask into global 3D coordinates and associate the obtained fused CLIP feature with the nearest 3D points in a pre-computed reference point cloud. Based on this association, we register the obtained segment features on a global point-wise feature map. The final point-wise features are then determined by averaging each reference point’s associated features. Based on the 3D segments obtained in the independent merging step, we can finally infer open-vocabulary vision-language features for all 3D segments as outlined in Fig. 2. In the subsequent step, we match point-wise features with the obtained 3D segments. For each point within a segment, we identify the nearest points in the reference point cloud and collect their CLIP features. Thus, we obtain a set of various CLIP features per 3D segment that is turned into a single segment-wise feature as follows: To mitigate potential high variance, instead of directly averaging these features, we employ DBSCAN clustering to handle cases like under-segmentation or imperfect views, ensuring a more representative feature by selecting the feature closest to the mean of the majority cluster.

B. 3D Scene Graph Construction

In this section, we describe how to build a hierarchical open-vocabulary scene graph given a global reference point

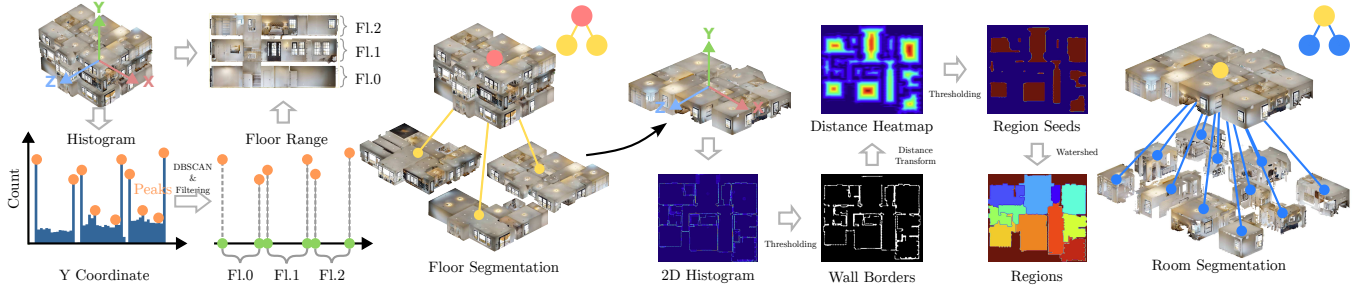


Fig. 3: Floor and Room Segmentation. Given the point cloud of the whole environment, floor and room nodes are subsequently derived based on geometric heuristics. Floor boundaries are computed by finding peaks of the pixel density along the height direction followed by filtering while room segment masks are extracted using the Watershed algorithm.

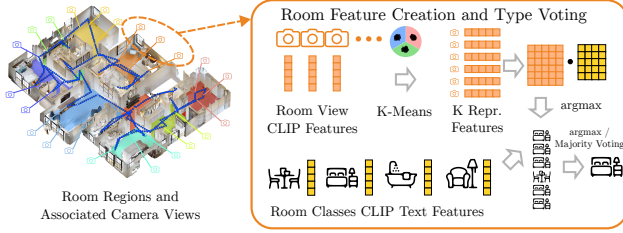


Fig. 4: By associating 10 camera views, i.e., its CLIP embeddings to each room we obtain a set of 10 open-vocabulary embeddings per segmented room. This serves as the attributed room feature in the scene graph.

cloud of the scene, a list of global 3D segments, and their associated CLIP features as described in Sec. III-A. We formalize our graph as $\mathcal{G} = (\mathcal{N}, \mathcal{E})$ where \mathcal{N} denotes the nodes and \mathcal{E} denotes the edges. The nodes can be expressed as $\mathcal{N} = \mathcal{N}_S \cup \mathcal{N}_F \cup \mathcal{N}_R \cup \mathcal{N}_O$, consisting of a root node \mathcal{N}_S , floor nodes \mathcal{N}_F , room nodes \mathcal{N}_R , and object nodes \mathcal{N}_O . Each node in the graph except the root node \mathcal{N}_S contains the point cloud of the concept it refers to and the open-vocabulary features associated with it. The edges can be written as $\mathcal{E} = \mathcal{E}_{SF} \cup \mathcal{E}_{FR} \cup \mathcal{E}_{RO}$. Here, \mathcal{E}_{SF} represents the edges between the root node and the floor nodes, \mathcal{E}_{FR} represents the edges between the floor nodes and the room nodes, and lastly, \mathcal{E}_{RO} denotes the edges between the room and object nodes.

1) *Floor Segmentation*: In order to separate floors, we identify peaks within a height histogram over all points contained in the point cloud. Given the point cloud of the whole environment, we construct the histogram over all points along the height axis using a bin size 0.01 m. Next, we identify peaks in this histogram (within a local range of 0.2 m) and select only peaks that exceed a minimum of 90% of the highest intensity peak. We apply DBSCAN and select the two highest-ranking peaks in each cluster. After that, every two consecutive values in the sorted height vector represent a single floor (floor and ceiling) in the building. The floor segmentation process is shown in Fig. 3. Using the obtained height levels, we can extract floor point clouds for each floor \mathcal{P}_l where l is the floor number. In addition, we equip each floor node with a CLIP text embedding using the template “floor {#}”. A graph edge between the root node and this floor node $(N_S, N_l) \in \mathcal{E}_{SF}$ is also established.

2) *Room Segmentation*: Based on each obtained floor point cloud, we construct a 2D bird’s-eye-view (BEV) histogram, from which the binary wall skeleton mask is extracted by thresholding the histogram. After dilating the wall mask and computing an Euclidean distance field (EDF), a number of isolated regions is derived by thresholding the EDF. Taking these regions as seeds, we apply the Watershed algorithm to obtain 2D region masks. The room segmentation process is further shown in Fig. 3. Given the 2D region masks, we extract the 3D points that fall into the floor’s height interval as well as the BEV room segment to form room point clouds that are used to associate objects to rooms later.

In order to attribute room nodes, we associate RGB-D observations whose camera poses reside within a room segment to those rooms, see Fig. 4. The CLIP embeddings of these images are filtered by extracting k representative view embeddings using the k-means algorithm. Given a list of room categories encoded via CLIP, we construct a cosine similarity matrix between the k representative features and all room category features. Next, we take the argmax along the category axis and obtain the most probable room type for each representative separately, resulting in k votes per room. Given these votes, we obtain the predicted room category by either taking the maximum-score vote or the majority vote across all k representatives per room.

These k representative embeddings and the room point cloud attribute the room node $N_{f,r}$, representing room r on floor f . An edge between the floor node and each room node $(N_f, N_{f,r}) \in \mathcal{E}_{FR}$ is established. The construction and querying of view embeddings are illustrated in Fig. 4.

3) *Object Identification*: Given the room point cloud, we associate object-level 3D segments that show a point cloud overlap with a potential candidate room in the bird’s-eye-view. Whenever a segment shows zero overlap with any room, we associate it with the room showing the smallest Euclidean distance. To reduce the number of nodes, we merge 3D segments of significant pair-wise partial overlap (Sec. III-A.1) that produce equal object labels when queried against a chosen label set. Each merged point cloud constitutes an object node $N_{f,r,o}$ that is connected to its corresponding room node $N_{f,r} \in \mathcal{N}_R$ by an edge $(N_{f,r}, N_{f,r,o}) \in \mathcal{E}_{RO}$. Each object node holds its corresponding 3D segment feature as described in Sec. III-A.1, its 3D segment point cloud

as well as a maximum-score object label for intermediate naming.

4) *Actionable Navigational Graph*: In addition to the open-vocabulary hierarchy, the scene graph also contains a navigational Voronoi graph that serves robotic traversability of the mapped surroundings [40] spanning multiple floors. This enables high-level planning and low-level execution based on the Voronoi graph. The creation of actionable graphs involves constructing per-floor and cross-floor navigation graphs. For the floor-level graph, the approach entails computing the free space map of the floor and creating a Voronoi graph [40] based on it. To construct per-floor graphs, we first obtain all camera poses and project them as 2D points onto a BEV map of each floor, assuming areas within a certain radius of each pose are pair-wise navigable. Subsequently, the entire floor’s region is obtained by projecting all floor-wise into the BEV plane. An obstacle map is generated based on points within a predefined height range $[y_{min} + \delta_1, y_{min} + \delta_2]$, where y_{min} is the minimal height of the floor points and δ_1, δ_2 are two thresholds we identify manually as $\delta_1 = 0.2$ and $\delta_2 = 1.5$. By taking the union of the pose region map and the floor region map and subtracting the obstacle region map, the free space map of each floor is derived. The Voronoi graph of this free map yields the floor graph. (See Fig. 5a). To build cross-floor navigation graphs, camera poses on stairs are connected to form a stairs-wise graph. Then, the closest nodes between the stairs graph and the floor-wise graph are selected and connected, completing the construction of cross-floor navigational graphs as shown in Fig. 5b.

C. Object Navigation from Long Queries

HOV-SG extends the scope of potential navigation goals to more specific spatial concepts like regions and floors compared to simple object goals [7], [10], [11], [16]. Language-guided navigation with HOV-SG involves processing complex queries such as “*find the toilet in the bathroom on floor 2*” using a large language model (GPT-3.5). We break down such lengthy instructions into three separate queries: one for the floor level, one for the room level, and one for the object level. Leveraging the explicit hierarchical structure of HOV-SG, we sequentially query against each hierarchy to progressively narrow down the solution space. This is done by taking the cosine similarity between the identified query floor, region and object as well as all objects, rooms and floors given in the graph, respectively. Once a target node is identified via scoring, we utilize the navigational graph mentioned above to plan a path from the starting pose to the target destination, which is demonstrated in Fig. S.1 and visualized in Fig. 1.

IV. EXPERIMENTAL EVALUATION

In the following, we first evaluate HOV-SG against recent open-vocabulary map representations on the task of 3D semantic segmentation on the ScanNet [41] and Replica datasets [42] in Sec. IV-A. In the same section, we justify the chosen approach by ablating several of our key contributions on the Replica dataset. Secondly, we investigate the accuracy of the constructed hierarchical, open-vocabulary 3D scene

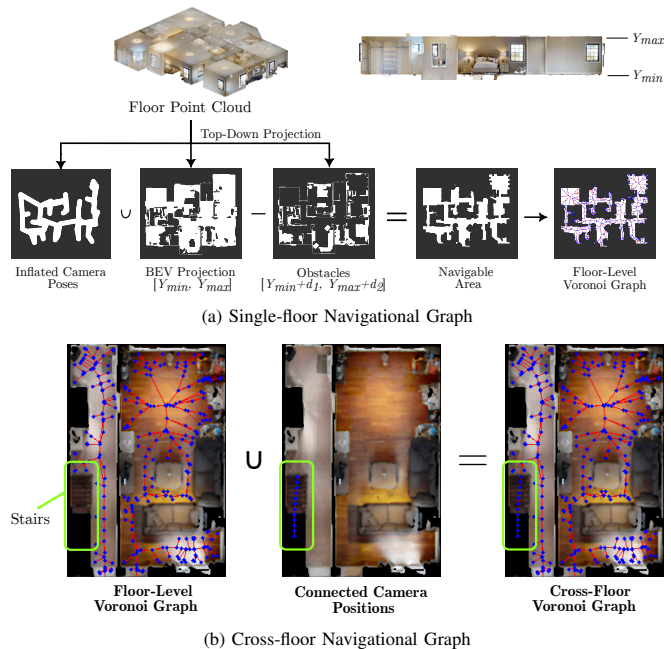


Fig. 5: Actionable Navigational Graph: The creation of the actionable navigational graph involves constructing single-floor and cross-floor navigational graphs: (a) By deducting the set of obstacles from the union of camera poses and the per-floor obtained BEV projection of the floor point cloud, we obtain the navigable area. Within this area we construct a Voronoi diagram as shown right. (b) In order to equip our navigational graph with cross-floor navigation capabilities, we extract the camera positions within regions classified as *stairs*. This subgraph is connected with the corresponding floor-level Voronoi graphs.

TABLE I: OPEN-VOCABULARY 3D SEMANTIC SEGMENTATION

Method	CLIP	Replica			ScanNet		
	Backbone	mIOU	F-mIOU	mAcc	mIOU	F-mIOU	mAcc
ConceptFusion [10]	OVSeg	0.10	0.21	0.16	0.08	0.11	0.15
	ViT-H-14	0.10	0.18	0.17	0.11	0.12	0.21
ConceptGraph [11]	OVSeg	0.13	0.27	0.21	0.15	0.18	0.23
	ViT-H-14	0.18	0.23	0.30	0.16	0.20	0.28
HOV-SG (ours)	OVseg	0.144	0.255	0.212	0.214	0.258	0.420
	ViT-H-14	0.231	0.386	0.304	0.222	0.303	0.431

Higher values are better. The ConceptFusion pipeline evaluated against made use of instance masks predicted by SAM [21]. We consider ViT-H-14 and a fine-tuned backbone ViT-L-14 released with the work OVSeg [39].

graphs on scenes of the Habitat Matterport 3D Semantics Dataset [43] (HM3DSem) in Sec. IV-B. Third, we study the open-vocabulary object retrieval capabilities of HOV-SG and demonstrate large-scale language-grounded robotic navigation in the real world (Sec. IV-C). In addition, we also compare the memory footprint of sparse and dense map representations in Sec. IV-D.

A. 3D Semantic Segmentation on ScanNet and Replica

We evaluate the open-vocabulary 3D semantic segmentation performance of HOV-SG on the ScanNet [41] and Replica [42] datasets. We compare our method with two competitive vision-and-language representations, namely ConceptFusion [10] and ConceptGraphs [11], and ablate over two CLIP backbones, see Table I. We consider the ViT-H-14 and a fine-tuned ViT-

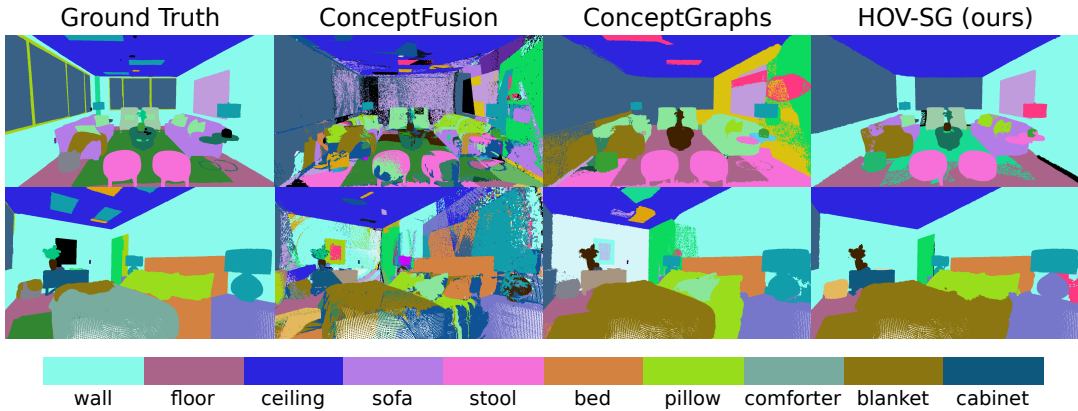


Fig. 6: Qualitative results for 3D semantic segmentation on the Replica dataset [42]

L-14 CLIP backbone released with the work OVSeg [39]. For each category in the dataset, we use the template: “There is the category in the scene.” and then generate its CLIP text embeddings [20] and the category name itself. Next, we average them to obtain the embedding of the specific category. We obtain predicted labels for each object node by computing the cosine similarity between all object nodes’ embeddings and all category embeddings and lastly apply the argmax operator.

Then we accumulate all objects’ point clouds to create our predicted point cloud \mathcal{P}_{pred} and transform the point cloud to the same coordinate frame as that of the point cloud with ground-truth (GT) semantic labels \mathcal{P}_{GT} . Given that the predicted point cloud may exhibit varying densities compared to the ground truth (GT), we iterate through each GT point to locate its five nearest points in \mathcal{P}_{pred} , and then determine the majority label among these points as the predicted label wrt. that respective GT point.

For consistency, we evaluate the same scenes evaluated in [10], [11]. For ScanNet, we evaluate scenes: scene0011_00, scene0050_00, scene0231_00, scene0378_00, scene0518_00. For Replica, we evaluate the following scenes: office0-office4 and room0-room2.

The semantic segmentation results on both Replica and ScanNet are shown in Tab. I. In terms of mIOU and F-mIOU, HOV-SG outperforms the open-vocabulary baselines by a large margin. This is primarily due to the following improvements we made: First, when we merge segment features, we consider all point-wise features that each segment covers and use DBSCAN to obtain the dominant feature, which increases the robustness compared to taking the mean as done by ConceptGraphs. Secondly, when we generate the point-wise features, we use the mask feature which is the weighted sum of the sub-image and its contextless counterpart. This mitigates the impact of salient background objects. Further qualitative results are shown in Fig. 6.

Ablation Study: In order to shed light on the contributions of various key components of our approach, we provide an ablation study on the Replica dataset [42] in Table II. One

TABLE II: ABLATION STUDY ON REPLICA

DBSCAN	L-CLIP	M-CLIP	mIOU \uparrow	F-mIoU \uparrow	mAcc \uparrow
\times	\checkmark	\checkmark	0.212	0.340	0.290
\checkmark	\times	\checkmark	0.136	0.178	0.170
\checkmark	\checkmark	\times	0.215	0.337	0.298
HOV-SG (ours)			0.231	0.386	0.304

DBSCAN indicates whether we apply DBSCAN clustering to select segment features, L-CLIP indicates the use of only masked images including background, and M-CLIP refers to only the masked CLIP embeddings without background.

key component of the 3D open-vocabulary segment-level mapping pipeline (Sec. III-A) is the DBSCAN clustering we apply to pixel-wise CLIP embeddings associated with each segment to select the most representative features among them. This design, inspired by the principle of majority voting, has proven effective in mitigating outlier CLIP features caused by the inherent limitations of CLIP and the noise originating from SAM’s outputs, thereby enhancing semantic accuracy. A different key component of our approach involves fusing CLIP features extracted from various sources: the global image, the masked image of an object based on its SAM mask, and the masked object image given the SAM mask without background. In contrast to ConceptGraphs [11], which only integrate the global image embedding and the sub-image embedding, we hypothesize that incorporating salient features from the sub-image into CLIP embeddings could enhance accuracy. Based on that, we tested three setups: utilizing only the CLIP embedding of the masked object including background (L-CLIP), employing only the CLIP embedding of the masked object without background (M-CLIP), and third, combining both of these CLIP embeddings by fusing them as done in HOV-SG. Our findings indicate that combining both embeddings yields the highest semantic accuracy as given in Table II.

B. Scene Graph Evaluation on Habitat 3D Semantics

In order to evaluate various aspects of the produced scene graph hierarchy, we have chosen the Habitat-Semantics dataset (HM3DSem) as it provides true open-vocabulary labels across large multi-floor scenes and also provides object-

region assignments. Since our approach operates on RGB-D frames, we manually record random walks of 8 scenes of the Habitat Semantics dataset [43], which span multiple rooms and floors: 00824, 00829, 00843, 00861, 00862, 00873, 00877, 00890. To construct ground-truth maps to compare against, we fuse the RGB-D and panoptic data across all frames given accurate odometry and obtain RGB and panoptic global ground truth. These maps are finally voxelized using a 0.02 cm resolution.

In the following, we analyze the floor and region segmentation performance in Sec. IV-B.1. In addition, we evaluate predicted region semantics (Sec. IV-B.2) as well as open-vocabulary object-level semantics (Sec. IV-B.3). In order to scrutinize the downstream capabilities of HOV-SG, we conduct two hierarchical object retrieval experiments given abstract language queries in Sec. IV-B.4. We display two exemplary constructed hierarchical 3D scene graphs in Fig. 8.

1) *Room and Floor Segmentation*: In order to evaluate both the floor and room segmentation performance, we identified several heuristics and augmented the provided metadata of HM3DSem. Since the dataset does not include floor height labels, we hand-labeled all upper and lower floor boundaries. In addition, we pooled the annotated objects contained in each of the ground-truth point clouds based on their associated region labels. Based on this, we obtain region-wise point clouds we utilize as ground truth. As shown in Table III, our method achieves a 100% success rate in retrieving the actual number of floors. Thus, the proposed heuristic achieves satisfactory results on both single-floor and multi-floor scenes. In addition, we evaluated the region segmentation performance of HOV-SG. Based on the protocol provided by Hydra [18], we evaluate the region precision and recall across 8 scenes on HM3DSem. The produced mean precision and recall are in line with the results provided by Hydra [18], although evaluated on a different set of scenes. In general, we obtain higher precision and recall on smaller scenes comprising fewer regions. Similar to Hydra, our approach utilizes a naïve morphological heuristic to segregate regions, which does not work well on more complex, semantically meaningful room layouts such as combined kitchen and living rooms. Nonetheless, our approach does not suffer from this drawback too drastically as we equip each segmented region with 10 representative embeddings. This allows adaptive prompting without directly setting a fixed room category.

2) *Semantic Room Classification*: We quantitatively support our proposed view embedding-based room category labeling method by comparing it against two strong baselines across 8 scenes on HM3DSem [43]. Both baselines rely on object labels to classify room categories. To draw a fair comparison, all methods rely on ground-truth room segmentation. Thus, objects are assigned to rooms based on ground-truth room layouts. This is done for the sake of comparability across different labeling methods. As a consequence, the considered room segmentations differ from the general HOV-SG method in this case.

TABLE III: Floor and Region Segmentation on HM3DSem

Method	Scene	Floors			Regions	
		Acc _F	#F _P	#F _{GT}	Precision	Recall
HOV-SG (ours)	00824	1.0	1	1	81.20	80.00
	00829	1.0	1	1	88.81	88.02
	00843	1.0	2	2	88.54	87.10
	00861	1.0	2	2	76.41	89.95
	00862	1.0	3	3	72.65	76.10
	00873	1.0	2	2	95.63	67.71
	00877	1.0	2	2	74.82	92.30
	00890	1.0	2	2	94.75	87.55
Overall	1.0	-	-	84.10	83.59	

Evaluation of the floor and room segmentation: We provide the number of correctly predicted floors using a threshold of 0.5m. Room segmentation precision (P) and recall (R) are calculated based on the metric provided by Hydra [18].

TABLE IV: SEMANTIC ROOM CLASSIFICATION RESULTS (HM3DSEM)

Room Identification Method	Acc ₌ [%]	Acc _≈ [%]
Privileged: GPT3.5 w/ GT obj. categories	66.89	81.49
Unprivileged: GPT3.5 w/ pred. obj. categories	28.48	42.95
HOV-SG w/ view embeddings (ours)	73.93	84.10

The table shows the room classification performance of our method (view embeddings) and two baselines (at the top) on HM3DSem. The baselines utilize GPT3.5 for labeling the rooms based on either ground-truth objects (masks) and categories or on predicted masks and categories. The Acc₌ metric measures whether the exact text-wise room category was predicted while Acc_≈ measures correct room labels based on qualitative human evaluation.

We utilize a closed set of room categories. To do so, we manually labeled the regions of the 8 scenes evaluated. The HM3DSem dataset does not provide annotated room categories but merely educated votes, which are often not sufficient. Thus, we will make the manual labels available as part of this work. The first and privileged baseline operates on ground-truth maps. This means that ground-truth rooms, objects (masks), and object categories are taken. In the next step, the baseline prompts GPT3.5 [44] to provide a room category guess (out of the closed set of room categories) based on the objects contained in each room [45]. The second and unprivileged baseline applies the same principle of prompting GPT3.5 but relies on the objects and masks obtained by HOV-SG. This means that object masks are imperfect and the top-1 predicted object category is taken to label objects. In general, we expect that the number of objects differs from the privileged baseline because of under- and over-segmentation of objects of HOV-SG. In comparison, our view embedding method relies on 10 distinct view embeddings, which are scored against the defined set of room categories. The final predicted room category is defined by the room category that showed the highest similarity across all view embeddings as described in Fig. 4.

We apply two different evaluation criteria: The first accuracy called Acc₌ fosters replicability by evaluating whether the predicted and the ground-truth room category are text-wise equal. Different from that, the performance regarding the Acc_≈ metric is produced via human evaluation. This is crucial as room categories are not always fully

TABLE V: OBJECT-LEVEL SEMANTICS EVALUATION ON HM3DSEM

Method	top_5	top_{10}	top_{25}	top_{100}	top_{250}	top_{500}	AUC_k^{top}
VLMs [7]	0.05	0.17	0.54	15.32	26.01	40.02	56.20
ConceptGraphs [11]	18.11	24.01	33.00	55.17	70.85	81.55	<u>84.07</u>
HOV-SG (ours)	18.43	25.73	36.41	56.46	69.95	80.86	84.88

We provide object-level semantic accuracies across all 8 considered scenes within HM3Dsem [43] using both the overall AUC_k^{top} metric across 1624 categories as well as accuracies at a few selected thresholds k .

determinable, especially for cases such as combined kitchen and living room areas. On top of that, the answers provided by GPT3.5 do not always state definitive categories because of frequent hallucinations. This is exacerbated by a high number of objects per room. This particularly applies to the unprivileged baselines when facing under-segmentation. In order to circumvent this, we manually review all predictions and check whether the LLM *leaned* towards the correct answer, meaning that we consider synonyms. For example, the Acc_{\approx} results consider “stairs” as correct even though the actual ground-truth label “staircase” was not predicted. This boosts results in favor of the LLM-based methods and is represented by the Acc_{\approx} metric.

As presented in Tab. IV, the view embedding method outperforms even the privileged baseline that relies on ground-truth object categories by $\sim 7\%$ wrt. the strict accuracy evaluation ($Acc_{=}$). We also observe a significant performance gap in terms of human evaluation, which is at 2.6%. There is only a single scene in which the privileged baseline outperforms our view embedding method (00877). The naïve baseline operating on predicted object categories is significantly outperformed, which is mostly due to under-segmentation and wrongly predicted top-1 object categories. Thus, we conclude that our method is robust and even outperforms privileged methods by a significant margin. We provide additional scene-wise results in the supplementary material Tab. S.1.

3) *Object-Level Semantics*: Existing open-vocabulary evaluations usually circumvent the problem of measuring true open-vocabulary semantic accuracy. This is due to arbitrary sizes of the investigated label sets, a potentially enormous amount of object categories [43], and the ease of use of existing evaluation protocols [7], [10]. While human-level evaluations solve this problem partly, robust replication of results remains challenging [11].

In this work, we propose the novel AUC_k^{top} metric that quantifies the area under the top- k accuracy curve between the predicted and the actual ground-truth object category. This entails computing the ranking of all cosine similarities between the predicted object feature and all possible category text features, which are in turn encoded using a vision-language model (CLIP). Thus, the metric encodes how many *erroneous shots* are necessary on average before the ground-truth label is predicted correctly. Based on this, the metric encodes the actual open-set similarity while scaling to large, variably-sized label sets. We envision a future use of this

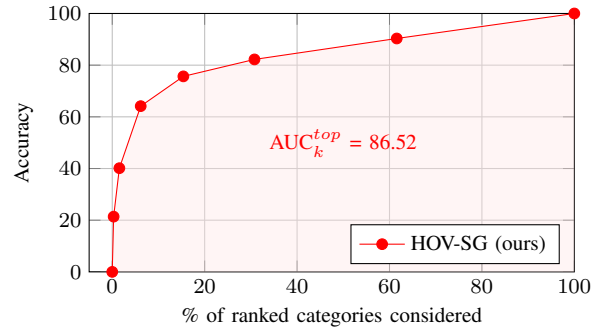


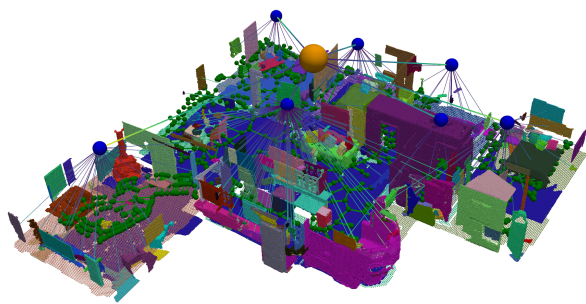
Fig. 7: We visualize the AUC_k^{top} curve for different evaluation thresholds k , which this plot measures in terms of percent out of the total number of categories (HM3Dsem: 1624). The shown curve represents the results of our method HOV-SG on the HM3Dsem scene 00824.

metric in diverse open-vocabulary tasks.

In order to show the applicability of the AUC_k^{top} metric, we compare HOV-SG against two strong baselines on the Habitat-Semantics dataset [43], which comprises an enormous label set of 1624 object categories. To allow for a fair comparison, we perform a linear assignment among predicted and GT objects and only consider predicted objects that show an $IoU > 50\%$ with the ground truth. Since VLMs [7] does not predict masks by design, it takes the masks predicted by HOV-SG and evaluates wrt. those. The overall AUC_k^{top} score as well as various top- k thresholds are given in Tab. V. We observe that VLMs [7] performs inferior, which is presumably due to its dense feature aggregation. It does not only score merely 5% of objects correctly given its top-5 choices but also only predicts the correct class given its top-500 predicted classes in 40.02% of all cases. In comparison, ConceptGraphs [11] obtains a competitive score of 84.07% while HOV-SG achieves 84.88%. Especially, up to the top-100 highest ranking classes, HOV-SG outperforms ConceptGraphs.

Furthermore, we visualize the AUC_k^{top} curve HOV-SG on the 00824 scene of HM3Dsem in Fig. 7. The closer the curve is to the upper left corner of the plot, the higher the open-vocabulary similarity. Instead of showing the accuracy at distinct values of k , we normalize k over the extent of the label set, which contains 1624 categories for HM3Dsem. This also shows visually how the AUC_k^{top} metric provides a dependable measure for large but variably-sized label sets.

4) *Hierarchical Concept Retrieval*: To take advantage of the hierarchical character of our proposed representation, we evaluate to what extent we can retrieve objects from hierarchical queries of the form: “pillow in the living room on the second floor” or “bottle in the kitchen”. To do so, we decompose the query using GPT-3.5 into its sought-after concepts and compute the corresponding CLIP embeddings. In the next step, we hierarchically query against the most suitable floor, the most appropriate room, and lastly, the most suitable object given the query at hand (see Tab. VI). While floor prompting is done naively, we select the room producing the highest maximum cosine similarity to the query room across its ten embeddings. On average, this produces higher



(a) Scene 00824 (single floor)



(b) Scene 00861 (2 floors)

Fig. 8: Qualitative visualization of the hierarchical 3D scene graphs produced by HOV-SG of two apartments of the Habitat Matterport 3D Semantics dataset [43]. Yellow nodes represent floors, while blue nodes represent rooms. The green graph right above the respective floor represents the produced navigational graph. For more visualizations, please refer to Fig. S.2.

TABLE VI: OBJECT RETRIEVAL FROM LANGUAGE QUERIES (HM3DSEM)

Query Type	Method	#Floors	#Regions	#Trials	SR ₁₀ [%]
(obj, room, floor)	ConceptGraphs	1.88	15.63	40.63	16.31
	HOV-SG (ours)				28.00
(obj, room)	ConceptGraphs	1.88	15.63	34.87	29.26
	HOV-SG (ours)				31.48

Evaluation of 20 frequent distinct object categories across 8 scenes. Success rate criterion: IoU > 0.1. The floor and room counts refer to the ground-truth labels. Floor, region, and trial counts are averaged across all scenes.

TABLE VII: REAL-WORLD RETRIEVAL AND NAVIGATION FROM LANGUAGE QUERIES

Query Type	# Trials	Graph Querying		Goal Navigation	
		# Successes	SR [%]	Success	SR [%]
Object	41	29	70.7	23	56.1
Room	9	5	55.6	5	55.6
Floor	2	2	100	2	100

We count a retrieval as successful whenever the robot is in close vicinity to the object sought after (~ 1 m).

success rates compared with mean- or median-based schemes.

In the following, we compare HOV-SG against an augmented variant of ConceptGraphs [11]. We equip it with privileged floor information while it scores objects against the requested room and object, which allows it to draw answers at the floor and room level. As shown in Tab. VI, HOV-SG shows a significant performance increase of 11.69% on object-room-floor queries and a 2.2% advantage on object-room queries when compared with ConceptGraphs. While ConceptGraphs struggles on larger scenes and under more detailed queries, HOV-SG outperforms it by a significant margin even though it suffers from erroneous room segmentations by design. For more information, we refer to Sec. S.2-B.

C. Real-World Experiments

To validate the system in the real world, we conduct multiple navigation trials using a Boston Dynamics *Spot* quadruped as shown in Fig. 9. First, we collect an RGB-D sequence of a two-story office building comprising a variety of room types as well as objects. Using this data, we create the hierarchical 3D scene graph presentations as introduced

in Sec. III above.

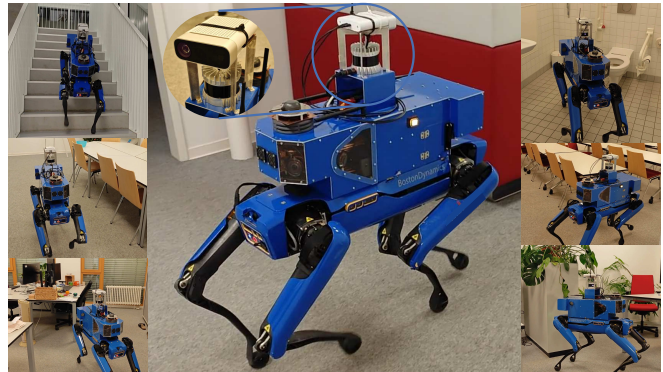


Fig. 9: Boston Dynamics *Spot* robot traversing a two-story office building with multiple types of rooms. The quadruped is equipped with an Azure Kinect RGB-D camera and a 3D LiDAR. We obtain accurate pose estimates from LiDAR-based odometry estimation.

We select 41 distinct object goals, 9 room goals, and 2 floor goals and use natural language to query the HOV-SG representation as detailed above. Some examples of the queries are “go to floor 0”, “navigate to the kitchen on floor 1”, or “find the plant in the office on floor 0”. Similar to the evaluation on Habitat-Semantics, we first evaluate general object retrieval given the scene graph. HOV-SG achieves a 100% success rate on floor retrieval, a 55.6% for room retrieval, and a 70.7% success rate for object retrieval. The major failure cases for room retrieval stem from the visual ambiguity among “meeting room”, “seminar room”, and “dining room”. Based on this, we evaluated the object navigation capabilities from abstract, hierarchical queries in the real world using the *Spot* quadruped. As detailed in Tab. VII, we observe a 56.1% success rate in object navigation while traversing multiple rooms as well as floors given an abstract long query. These results prove the efficacy of HOV-SG in enabling real-world agents to navigate to language-conditioned goals across multiple floors. We display three trials in more detail in the supplementary material Fig. S.3.

TABLE VIII: REPRESENTATION SIZE (HM3DSEM)

Scene	# Floors	VLMaps [7]	ConceptGraphs [11]	HOV-SG (ours)
00824	1	568	143	143
00829	1	407	110	99
00843	2	534	143	125
00861	2	943	255	225
00862	3	1808	474	479
00873	2	570	167	129
00877	2	556	154	131
00890	2	682	192	162
Σ	-	6068	1638	1493

We compare the storage sizes of the representations produced by VLMaps [7], ConceptGraphs [11], and HOV-SG (ours), measured in megabyte (MB), across 8 differently sized scenes of Habitat-Semantics (HM3DSem). The smallest sizes are highlighted **bold**, respectively.

D. Representation Storage Overhead Evaluation

A key advantage of HOV-SG is the compactness of the representation. We compare the sizes of VLMaps [7], ConceptGraphs [11], and HOV-SG created for the eight scenes in the HM3DSem dataset and show the results in Tab. VIII. We adapt VLMaps to store LSeg features at 3D voxel locations. The backbone of the LSeg is ViT-B-32, which has 512 dimensional features. ConceptGraphs and HOV-SG are using the ViT-H-14 CLIP backbones, which requires saving 1024-dimension features in the representation. VLMaps is optimized to only save features at voxels near object surfaces instead of saving redundant features at non-occupied voxels. Nonetheless, thanks to the compact graph structure, ConceptGraphs and HOV-SG are much smaller than their dense counterparts. HOV-SG even reduces as much as 75% in memory footprint on average compared to VLMaps. When ConceptGraphs encodes supplementary object relationship information within their graphs, HOV-SG incorporates hierarchical semantic features that are lacking in other representations. Overall, ConceptGraphs and HOV-SG serve as excellent complementary representations, each emphasizing distinct facets of scene semantics.

V. CONCLUSION

We presented HOV-SG, a hierarchical open-vocabulary 3D scene graphs representation for robot navigation. Through the semantic decomposition of environments into floors, rooms, and objects, we demonstrate effective concept retrieval from abstract language queries and perform long-horizon navigation across a multi-story environment in the real world. With extensive experiments conducted across multiple datasets, we showcase that HOV-SG surpasses previous baselines in terms of semantic accuracy, open-vocabulary capability, and compactness. Nevertheless, HOV-SG is not without limitations. Consisting of several stages and components, our approach necessitates a large number of hyper-parameters. Moreover, the construction process of HOV-SG is time-consuming, rendering the method unsuitable for real-time mapping. Furthermore, it assumes a static environment and thus cannot handle dynamic environments. Future research directions may involve developing an open-vocabulary dynamic

representation of the environment or integrating a reactive embodied agent to enhance reasoning and grounding in the physical world.

REFERENCES

- [1] E. Jefferies and X. Wang, "Semantic cognition: semantic memory and semantic control," in *Oxford Research Encyclopedia of Psychology*, 2021.
- [2] A. A. Kumar, "Semantic memory: A review of methods, models, and current challenges," *Psychonomic Bulletin & Review*, vol. 28, pp. 40–80, 2021.
- [3] S. C. Hirtle and J. Jonides, "Evidence of hierarchies in cognitive maps," *Memory & cognition*, vol. 13, no. 3, pp. 208–217, 1985.
- [4] B. Kuipers, "The spatial semantic hierarchy," *Artificial Intelligence*, vol. 119, no. 1, pp. 191–233, 2000.
- [5] H. Voicu, "Hierarchical cognitive maps," *Neural Networks*, vol. 16, no. 5-6, pp. 569–576, 2003.
- [6] D. Shah, B. Osiński, S. Levine, *et al.*, "Lm-nav: Robotic navigation with large pre-trained models of language, vision, and action," in *Conf. on Robot Learning*. PMLR, 2023, pp. 492–504.
- [7] C. Huang, O. Mees, A. Zeng, and W. Burgard, "Visual language maps for robot navigation," in *Int. Conf. on Robotics and Automation*, London, UK, 2023.
- [8] B. Chen, F. Xia, B. Ichter, K. Rao, K. Gopalakrishnan, M. S. Ryoo, A. Stone, and D. Kappler, "Open-vocabulary queryable scene representations for real world planning," in *Int. Conf. on Robotics and Automation*. IEEE, 2023, pp. 11 509–11 522.
- [9] N. M. M. Shafiqullah, C. Paxton, L. Pinto, S. Chintala, and A. Szlam, "Clip-fields: Weakly supervised semantic fields for robotic memory," *arXiv preprint arXiv: Arxiv-2210.05663*, 2022.
- [10] K. M. Jatavallabhula, A. Kuwajerwala, Q. Gu, M. Omama, T. Chen, S. Li, G. Iyer, S. Saryazdi, N. Keetha, A. Tewari, *et al.*, "Conceptfusion: Open-set multimodal 3d mapping," *Robotics: Science and Systems*, 2023.
- [11] Q. Gu, A. Kuwajerwala, S. Morin, K. Jatavallabhula, B. Sen, A. Agarwal, C. Rivera, W. Paul, K. Ellis, R. Chellappa, C. Gan, C. de Melo, J. Tenenbaum, A. Torralba, F. Shkurti, and L. Paull, "Conceptgraphs: Open-vocabulary 3d scene graphs for perception and planning," *arXiv*, 2023.
- [12] O. Mees, J. Borja-Diaz, and W. Burgard, "Grounding language with visual affordances over unstructured data," in *Int. Conf. on Robotics and Automation*. IEEE, 2023, pp. 11 576–11 582.
- [13] J. Wu, R. Antonova, A. Kan, M. Lepert, A. Zeng, S. Song, J. Bohg, S. Rusinkiewicz, and T. Funkhouser, "Tidybot: Personalized robot assistance with large language models," *Autonomous Robots*, 2023.
- [14] S. Thrun, W. Burgard, and D. Fox, *Probabilistic Robotics*. MIT Press, 2005.
- [15] E. Greve, M. Büchner, N. Vödisch, W. Burgard, and A. Valada, "Collaborative dynamic 3d scene graphs for automated driving," *arXiv preprint arXiv:2309.06635*, 2023.
- [16] C. Huang, O. Mees, A. Zeng, and W. Burgard, "Audio visual language maps for robot navigation," in *Int. Symposium. on Experimental Robotics*, Chiang Mai, Thailand, 2023.
- [17] S. Peng, K. Genova, C. M. Jiang, A. Tagliasacchi, M. Pollefeys, and T. Funkhouser, "Openscene: 3d scene understanding with open vocabularies," in *Proc. of the IEEE Conf. on Computer Vision and Pattern Recognition*, 2023.
- [18] N. Hughes, Y. Chang, and L. Carlone, "Hydra: A real-time spatial perception system for 3D scene graph construction and optimization," in *Robotics: Science and Systems*, 2022.
- [19] A. Rosinol, A. Gupta, M. Abate, J. Shi, and L. Carlone, "3D dynamic scene graphs: Actionable spatial perception with places, objects, and humans," *Robotics: Science and Systems*, 2020.
- [20] A. Radford, J. W. Kim, C. Hallacy, A. Ramesh, G. Goh, S. Agarwal, G. Sastry, A. Askell, P. Mishkin, J. Clark, *et al.*, "Learning transferable visual models from natural language supervision," in *Int. Conf. on Machine Learning*. PMLR, 2021, pp. 8748–8763.
- [21] A. Kirillov, E. Mintun, N. Ravi, H. Mao, C. Rolland, L. Gustafson, T. Xiao, S. Whitehead, A. C. Berg, W.-Y. Lo, P. Dollar, and R. Girshick, "Segment anything," in *Int. Conf. on Computer Vision*, October 2023, pp. 4015–4026.
- [22] M. Chang, T. Gervet, M. Khanna, S. Yenamandra, D. Shah, S. Y. Min, K. Shah, C. Paxton, S. Gupta, D. Batra, *et al.*, "Goat: Go to any thing," *arXiv preprint arXiv:2311.06430*, 2023.

- [23] S. Y. Gadre, M. Wortsman, G. Ilharco, L. Schmidt, and S. Song, “Cows on pasture: Baselines and benchmarks for language-driven zero-shot object navigation,” in *Proc. of the IEEE Conf. on Computer Vision and Pattern Recognition*, 2023, pp. 23 171–23 181.
- [24] Ó. M. Mozos, C. Stachniss, A. Rottmann, and W. Burgard, “Using adaboost for place labeling and topological map building,” in *Int. Symposium of Robotics Research*. Springer, 2007, pp. 453–472.
- [25] R. F. Salas-Moreno, R. A. Newcombe, H. Strasdat, P. H. Kelly, and A. J. Davison, “Slam++: Simultaneous localisation and mapping at the level of objects,” in *Proc. of the IEEE Conf. on Computer Vision and Pattern Recognition*, 2013, pp. 1352–1359.
- [26] M. Grinvald, F. Furrer, T. Novkovic, J. J. Chung, C. Cadena, R. Siegwart, and J. Nieto, “Volumetric instance-aware semantic mapping and 3d object discovery,” *IEEE Robotics and Automation Letters*, vol. 4, no. 3, pp. 3037–3044, 2019.
- [27] J. McCormac, R. Clark, M. Bloesch, A. Davison, and S. Leutenegger, “Fusion++: Volumetric object-level slam,” in *Int. Conf. on 3D Vision*. IEEE, 2018, pp. 32–41.
- [28] B. Xu, W. Li, D. Tzoumanikas, M. Bloesch, A. Davison, and S. Leutenegger, “Mid-fusion: Octree-based object-level multi-instance dynamic slam,” in *Int. Conf. on Robotics and Automation*. IEEE, 2019, pp. 5231–5237.
- [29] L. Nicholson, M. Milford, and N. Sünderhauf, “Quadricslam: Dual quadrics from object detections as landmarks in object-oriented slam,” *IEEE Robotics and Automation Letters*, vol. 4, no. 1, pp. 1–8, 2018.
- [30] S. Yang and S. Scherer, “Cubeslam: Monocular 3-d object slam,” *IEEE Transactions on Robotics*, vol. 35, no. 4, pp. 925–938, 2019.
- [31] J. Kerr, C. M. Kim, K. Goldberg, A. Kanazawa, and M. Tancik, “Lerf: Language embedded radiance fields,” in *Proc. of the IEEE Conf. on Computer Vision and Pattern Recognition*, 2023, pp. 19 729–19 739.
- [32] I. Armeni, Z.-Y. He, A. Zamir, J. Gwak, J. Malik, M. Fischer, and S. Savarese, “3D scene graph: A structure for unified semantics, 3D space, and camera,” in *Int. Conf. on Computer Vision*, 2019, pp. 5663–5672.
- [33] S.-C. Wu, J. Wald, K. Tateno, N. Navab, and F. Tombari, “Scene-GraphFusion: Incremental 3D scene graph prediction from RGB-D sequences,” in *Proc. of the IEEE Conf. on Computer Vision and Pattern Recognition*, June 2021, pp. 7515–7525.
- [34] K. Rana, J. Haviland, S. Garg, J. Abou-Chakra, I. Reid, and N. Suen-derhauf, “Sayplan: Grounding large language models using 3d scene graphs for scalable task planning,” in *Conf. on Robot Learning*, 2023.
- [35] D. Honerkamp, M. Buchner, F. Despinoy, T. Welschhold, and A. Valada, “Language-grounded dynamic scene graphs for interactive object search with mobile manipulation,” *arXiv preprint arXiv:2403.08605*, 2024.
- [36] H. Bavlle, J. L. Sanchez-Lopez, M. Shaheer, J. Civera, and H. Voos, “Situational graphs for robot navigation in structured indoor environments,” *IEEE Robotics and Automation Letters*, vol. 7, no. 4, pp. 9107–9114, 2022.
- [37] R. Kümmerle, G. Grisetti, H. Strasdat, K. Konolige, and W. Burgard, “G2o: A general framework for graph optimization,” in *Int. Conf. on Robotics and Automation*, 2011, pp. 3607–3613.
- [38] J. Wald, H. Dharmo, N. Navab, and F. Tombari, “Learning 3d semantic scene graphs from 3d indoor reconstructions,” in *Proc. of the IEEE Conf. on Computer Vision and Pattern Recognition*, 2020.
- [39] F. Liang, B. Wu, X. Dai, K. Li, Y. Zhao, H. Zhang, P. Zhang, P. Vajda, and D. Marculescu, “Open-vocabulary semantic segmentation with mask-adapted clip,” in *Proc. of the IEEE Conf. on Computer Vision and Pattern Recognition*, 2023, pp. 7061–7070.
- [40] S. Thrun and A. Bücken, “Integrating grid-based and topological maps for mobile robot navigation,” in *Proc. of the AAAI Conference on Artificial Intelligence (AAAI)*, 1996.
- [41] A. Dai, A. X. Chang, M. Savva, M. Halber, T. Funkhouser, and M. Nießner, “ScanNet: Richly-annotated 3d reconstructions of indoor scenes,” 2017, pp. 5828–5839.
- [42] J. Straub, T. Whelan, L. Ma, Y. Chen, E. Wijmans, S. Green, J. J. Engel, R. Mur-Artal, C. Ren, S. Verma, *et al.*, “The replica dataset: A digital replica of indoor spaces,” *arXiv preprint arXiv:1906.05797*, 2019.
- [43] K. Yadav, R. Ramrakhya, S. K. Ramakrishnan, T. Gervet, J. Turner, A. Gokaslan, N. Maestre, A. X. Chang, D. Batra, M. Savva, *et al.*, “Habitat-matterport 3d semantics dataset,” in *Proc. of the IEEE Conf. on Computer Vision and Pattern Recognition*, 2023, pp. 4927–4936.
- [44] R. OpenAI, “Gpt-4 technical report,” *arXiv*, pp. 2303–08 774, 2023.
- [45] W. Chen, S. Hu, R. Talak, and L. Carlone, “Leveraging large language models for robot 3d scene understanding,” *arXiv preprint arXiv:2209.05629*, 2022.

Hierarchical Open-Vocabulary 3D Scene Graphs for Language-Grounded Robot Navigation

- Supplementary Material -

Abdelrhman Werby^{1*}, Chenguang Huang^{1*}, Martin Büchner^{1*}, Abhinav Valada¹, and Wolfram Burgard²

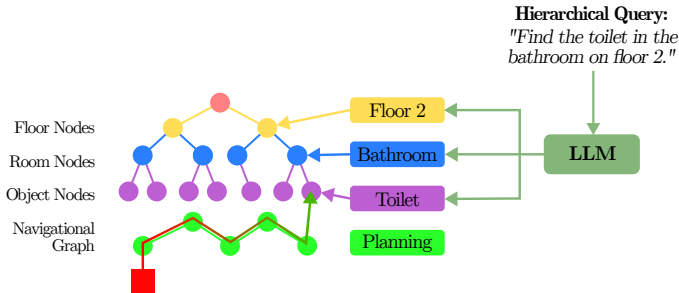


Fig. S.1: The language-grounded navigation module of HOV-SG allows to parse complex queries such as “find the toilet in the bathroom on floor 2” into three queries using a large language model (GPT-3.5) - one each for the floor, room, and object levels. Leveraging HOV-SG’s hierarchical structure, we progressively narrow down the search space by querying at each level. Once the target location is identified, the action graph in HOV-SG is used to plan a path from the starting pose to the target.

In this supplementary material, we expand upon multiple aspects of our main paper. In Sec. S.1, we detail the semantic localization scheme. In Sec. S.2, we additionally present experimental results that support the claims introduced in the manuscript. This includes a more detailed discussion of the proposed open-vocabulary metric, an analysis regarding identified semantic room categories, and additional baselines regarding object retrieval from language queries. Moreover, we provide insightful visualizations of the produced multi-story scene graphs, representing scenes from both Habitat Semantics (HM3DSem) [43] as well as our real-world environment.

S.1. METHOD DETAILS

A. Semantic Localization

HOV-SG achieves agent localization within the graph using only RGB images and local odometry using a simple particle filter. The process involves randomly initializing K particles within the free space map, estimated from each floor’s point cloud. Subsequently, the global CLIP feature of the RGB image and the CLIP feature of objects within the image are extracted using the same pipeline as used for the graph creation. In the prediction step, the particle poses are updated based on robot odometry. Thus, we assign each particle a floor and room based on its updated coordinates. In the update step,

we calculate cosine similarity scores between the current RGB image’s global CLIP feature and the graph’s room features for each particle. Additionally, scores are computed between object features in the RGB image and observed objects in front of each particle. Then, particle weights are adjusted based on these similarity scores. This integrated approach allows HOV-SG to semantically localize the agent within the graph at the floor and room level within a short span of 10 observed frames.

S.2. EXPERIMENTAL EVALUATION

A. Room Classification

We support the average numbers provided in the main manuscript with scene-wise results in Tab. S.1.

TABLE S.1: Semantic Room Classification Results (HM3DSem).

Room Identification Method	Scene	Acc ₌ [%]	Acc _≈ [%]
GPT3.5 w/ ground-truth object categories (privileged)	00824	70.00	90.00
	00829	71.43	100.00
	00842	61.54	69.23
	00861	58.33	70.83
	00862	50.00	72.22
	00873	81.82	90.91
	00877	69.23	76.92
	00877	72.73	81.82
	<i>Overall</i>	<u>66.89</u>	<u>81.49</u>
GPT3.5 w/ predicted object categories (unprivileged)	00824	30.00	40.00
	00829	42.86	57.14
	00842	38.46	38.46
	00861	16.67	25.00
	00862	19.44	25.00
	00873	45.45	63.64
	00877	07.69	30.77
	00877	27.27	63.64
	<i>Overall</i>	28.48	42.95
View embeddings (ours)	00824	80.00	90.00
	00829	85.71	100.00
	00842	69.23	76.92
	00861	54.17	79.17
	00862	63.89	83.33
	00873	90.91	90.91
	00877	61.54	61.54
	00877	81.82	90.91
	<i>Overall</i>	73.93	84.10

We show the room classification performance of our method (view embeddings) and two baselines (at the top) on HM3DSem. The baselines utilize GPT3.5 for labeling the rooms based on either ground-truth objects (masks) and categories or on predicted masks and categories. We consider two different evaluation criteria: Acc₌ measures whether the exact text-wise room category was predicted while Acc_≈ measures correct room labels based on qualitative human evaluation.

*These authors contributed equally.

¹Department of Computer Science, University of Freiburg, Germany.

²Department of Eng., University of Technology Nuremberg, Germany

TABLE S.2: Object Retrieval from Language Queries (HM3DSem).

Query Type	Method	Scene	#Floors	#Regions	#Trials	SR ₁₀ [%]
(o, r, f)	ConceptGraphs	00824	1	10	33	33.33
		00829	1	7	20	65.00
		00843	2	13	26	03.85
		00861	2	24	55	01.82
		00862	3	36	90	21.11
		00873	2	11	28	10.71
		00877	2	13	32	09.38
		00890	2	11	41	04.88
		Overall	-	-	40.63	16.31
	(o, r)	HOV-SG (ours) w/ OVSeg	00824	1	10	33
00829			1	7	20	45.00
00843			2	13	26	34.62
00861			2	24	55	25.45
00862			3	36	90	21.11
00873			2	11	28	14.29
00877			2	13	32	25.00
00890			2	11	41	21.95
Overall			-	-	40.63	28.00
(o, r)		ConceptGraphs	00824	1	10	33
	00829		1	7	20	65.00
	00843		2	13	23	34.78
	00861		2	24	46	19.57
	00862		3	36	67	26.98
	00873		2	11	25	30.00
	00877		2	13	24	25.00
	00890		2	11	41	21.95
	Overall		-	-	34.88	29.26
	(o, r)	HOV-SG (ours)	00824	1	10	33
00829			1	7	20	45.00
00843			2	13	23	39.13
00861			2	24	46	30.43
00862			3	36	67	20.63
00873			2	11	25	20.00
00877			2	13	24	33.33
00890			2	11	41	21.95
Overall			-	-	34.88	31.48

Evaluation over 20 frequent distinct object categories in terms of the top-5 accuracy. A match is counted as a success when the IoU > 0.1 between predicted object and ground truth. The floor and room counts refer to the ground-truth labels. The number of trials is lower for (o, r) compared to (o, r, f) because we observe a higher number of query duplicates whenever we drop the floor specification. The 20 categories evaluated are: *picture, pillow, door, lamp, cabinet, book, chair, table, towel, plant, sink, stairs, bed, toilet, tv, desk, couch, flowerpot, nightstand, faucet*.

B. Language-Grounded Navigation with Long Queries

In order to support our proposed hierarchical segregation of the environment, we present another comparison with ConceptGraphs [11]. To do so, we compare the object retrieval from language queries performance to demonstrate the efficacy of hierarchically decomposing scenes. We draw this comparison by augmenting ConceptGraphs to also work with room and floor queries. For both HOV-SG as well as ConceptGraphs, we decompose the original query via GPT3.5 parsing as before. Using this, we obtain text variables stating the requested floor name, room name, and object name. Since the floor segmentation of HOV-SG consistently showed 100% accuracy, we directly provide ConceptGraphs with that information. Our augmentation of ConceptGraphs allows us to implicitly identify potential target rooms and objects: We compute the cosine similarity between the set of all object embeddings and the queried room text. Similarly, we compute the cosine similarity between the set of all objects and the queried object name. We combine these two similarities by

taking the product of those scores per object to identify the most probable objects. This allows ConceptGraphs to draw answers at the floor level and room level. The remaining details of this evaluation are detailed in the main manuscript.

The results in Tab. S.2 regarding object-room-floor queries demonstrate a significant performance improvement of 11.69% when using HOV-SG compared to ConceptGraphs. We observe that ConceptGraphs struggles with larger scenes and under-segmentation of the produced maps, which often makes finding the object in question hard. Regarding the object-room queries, the drawbacks of ConceptGraphs are not as apparent because the search domain is significantly larger. Still, HOV-SG shows a 2.2% advantage over ConceptGraphs. In general, erroneous room segmentations produced by HOV-SG make finding the object in question hard, which remains subject to future work.

C. Graph Representation on HM3DSem

In the following, we also show the 6 additional hierarchical 3D scene graphs we evaluated in Fig. S.2. Each distinct object is colored with a different color and the ground truth floor surface is underlayed for easier visibility. The blue nodes denote rooms and its links to the objects denote the object-room associations. The edges among the yellow nodes and the blue nodes show the association between rooms and floors. For clear visualization, we do not visualize the root node that connects multiple floors. We reject certain objects for visualization based on their top-1 predicted object category (out of 1624 categories). Any categories containing substrings of the following have not been visualized: wall, floor, ceiling, paneling, banner, overhang. All other predicted object categories are shown. Remarkably, this procedure removed the fair majority of ceilings, walls, etc., which confirms the accuracy of the top-1 predicted open-vocabulary object labels. Nonetheless, future work should address the problem of over- and under-segmentation in these maps. Coping with multiple overlapping masks produced during iterative mask merging is still an open question. While having multiple overlapping masks per point drives the recall in semantic retrieval, this does not produce visually appealing maps. In general, one could argue that depending on the language query at hand different concepts are requested. In case of a query such as “Find the sofa”, one would like to obtain the mask that encloses the whole sofa. On the other hand, if the query comes in the form of “Find the cushion” (on the sofa), we would want to singulate the cushion in question. This however is difficult when the sofa is masked as one, which would then be considered under-segmentation. Thus, we envision maps that can hold multiple overlapping object masks that could represent various sub-concepts. Essentially, this translates to an additional object hierarchy layer that decomposes objects into their parts.

D. Real-World Environment

In Fig. S.3, we present three real-world trials that were executed with a Boston Dynamics Spot quadrupedal robot, which allowed us to traverse multi-floor environments safely,

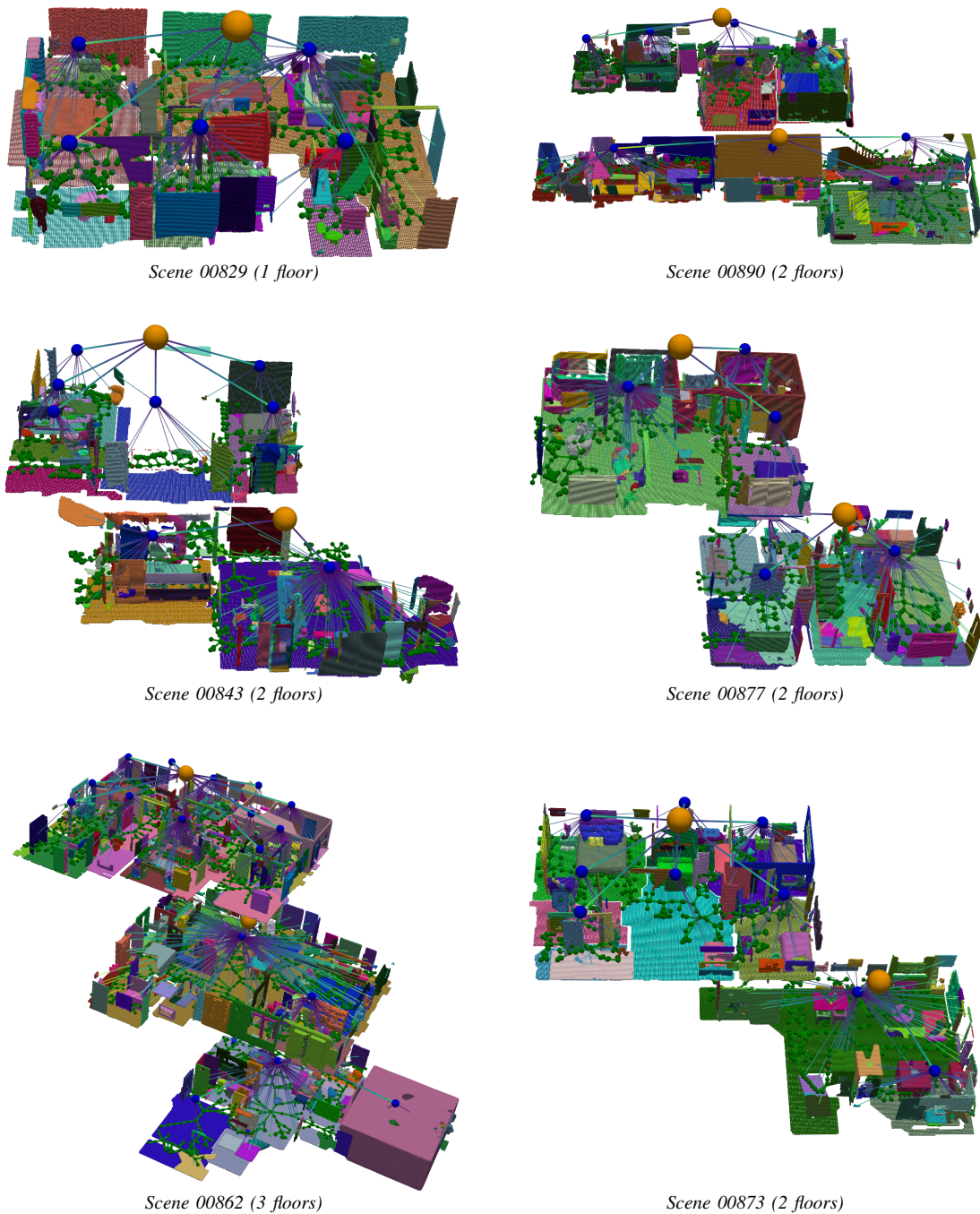
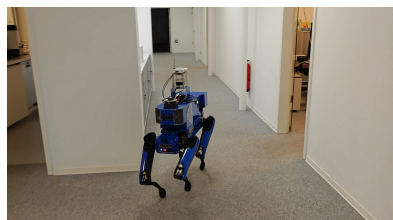
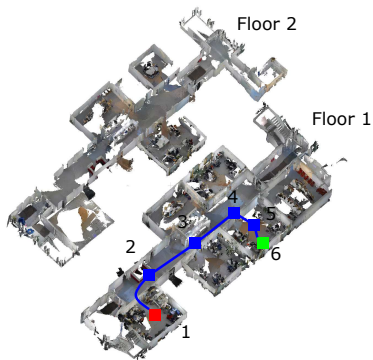


Fig. S.2: We show a visualization of the hierarchical open-vocabulary scene graphs produced on HM3Dsem. To make the visualization more clear we do not show the root node connecting (multiple) floors. In addition, we underlay the ground-truth floor surface for easier visibility. We reject certain objects for visualization based on their top-1 predicted object category (out of 1624 categories). Any categories containing sub-strings of the following have not been visualized: wall, floor, ceiling, paneling, banner, overhang. All other predicted object categories are shown. Remarkably, this procedure removed the fair majority of ceilings, walls, etc., which confirms the accuracy of the top-1 predicted open-vocabulary object labels. Best viewed zoomed in.

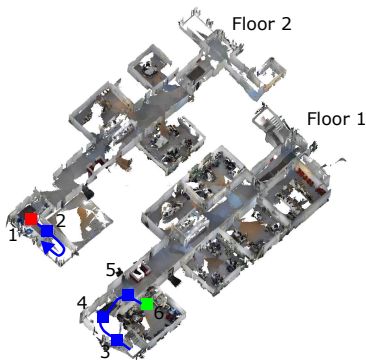
see Fig. 9. The trials are performed based on complex hierarchical language queries that specify the floor, the room, and the object to find. All hierarchical concepts relied on in these experiments are identified using our open-vocabulary HOV-SG pipeline. The top row in Fig. S.3 shows the taken path (blue) from the start position (red) to the goal location (green). The following rows show the time-wise progression

of the trial from top to bottom. The unique difficulty in these experiments is the typical office/lab environment with many similar rooms, which often produced similar room names. Having semantically varied rooms instead drastically simplifies these tasks. Nonetheless, as reported in the main manuscript, we reach real-world success rates of around 55%.

“Find the bean bag in the office on floor 1”



“Find the coat in the office on floor 1”



“Find the toilet in the bathroom on floor 2”

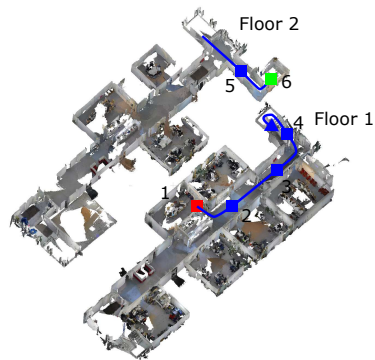


Fig. S.3: Real-World Object Navigation from Language Queries: We show a set of qualitative results of the real-world demonstration trials, which uses a Boston Dynamics Spot to allow for multi-floor traversals. The first row displays the observed scene and the taken path from the start (red) to the goal location (green). The following rows detail the time-wise progression (top-to-bottom).